ELSEVIER

Transient heat transfer to a spheroidal liquid drop suspended in an electric field

M. A. Jog and M. A. Hader
Department of Mechanical, Industrial, and Nuclear Engineering, University of Cincinnati, Cincinnati, Ohio

Heat transfer to a spheroidal drop of a dielectric fluid suspended in another dielectric fluid in the presence of an electric field is investigated in this paper. The effect of drop deformation on the heat transport is analyzed. A range of prescribed drop deformations from $b/a=0.99$ to $b/a=0.4$ is considered. The electric potential distribution is numerically obtained for each deformed drop configuration. The resulting flow field is determined by the solution of the Navier–Stokes equations in the continuous and the dispersed phase. The transient heat transfer is studied in the limit of bulk of the resistance to the heat transport being in the droplet. An alternating-direction-implicit (ADI) method is used to obtain the transient temperature field for drop Peclet number from 5 to 1500. In the limiting case of negligible drop deformation, we recover the flow field and the electrically induced interfacial stresses for a liquid sphere calculated by analytical methods. Heat transfer results for a spherical drop ($b/a=0.99$) show excellent agreement with results available in the published literature. Study of drop deformation reveals interesting features in the flow and heat transport. The location of the maximum surface velocity moves toward the equatorial plane for a deformed drop compared to that for a liquid sphere. It is found that the increase in drop deformation results in higher steady state Nusselt numbers for very large as well as very small equivalent Peclet numbers. However, for intermediate equivalent drop Peclet numbers, the equivalent steady state Nusselt numbers for a deformed drop may be lower than for a sphere.

Keywords: liquid drop; heat transfer enhancement; electric field; numerical analysis

Introduction

Direct-contact heat/mass transfer from liquid drops in a uniform electric field has received considerable attention in the context of enhancement of heat/mass transport. Taylor (1966) studied flow and deformation of a drop of a leaky dielectric fluid suspended in another fluid. He showed that the interfacial stresses caused by the presence of the electric field produce a circulatory motion inside the drop. Oliver et al. (1985) analyzed the heat transfer to a spherical liquid drop suspended in an electric field. They showed that, for large Peclet numbers, the Nusselt number for purely electrically driven flow becomes increasingly independent of the Peclet number. The maximum steady-state Nusselt number in the limit of large Peclet number was shown to be around 30. This value is significantly higher than 17.9, the Nusselt number for a drop translating in gravitational field in the absence of an electric field (Clift et al. 1978). The exact value of the maximum Nusselt number for a suspended drop in a uniform electric field is shown to be 29.8 by Oliver and DeWitt (1993). Advances made in the analysis of heat/mass transport from liquid drops in the presence of an electric field are available in a recent detailed review by Ayyaswamy (1995) and are not discussed here for brevity.

Heretofore, the studies of heat/mass transport from a liquid drop in a uniform electric field have considered the drop shape to be spherical. For a moving drop, in the absence of electric field, the assumption of sphericity is appropriate if the Weber number and the Eötvös numbers are small (Sadhal and Johnson 1986; Jog et al. 1996). However, for a drop suspended in a uniform electric field, drop deformations are possible even for small Eötvös numbers. This is because of the presence of nonuniform normal stresses induced by the electric field. Only for certain specific combination of the electrothermophysical properties of the dispersed and the continuous phase the drop may remain spherical (Taylor 1966). Under these conditions, the viscous stresses normal to the drop surface attributable to the induced circulatory flow exactly cancel the effect of the normal stress variation caused by the electric field. In general, the nonuniformity in the normal stress at the drop surface leads to deformation of the drop. As a drop deforms, the electric field at the drop surface changes, and the electrically induced surface stresses are altered (Feng and Scott 1996). This results in a change in the flow field in the dispersed and the continuous phase. Consequently, deformation of a drop can significantly impact the heat transport characteristics. A computational model to calculate drop deformations under the influence of electric field has been recently reported by Feng and Scott (1996). They found that the field strength usually exhibits a turning point

Address reprint requests to Dr. M. A. Jog, Dept. of Mechanical, Industrial, and Nuclear Engineering, University of Cincinnati, Cincinnati, OH 45221-0072, USA.

Received 27 June 1996; accepted 30 August 1996

Int. J. Heat and Fluid Flow 18: 411–418, 1997

655 Avenue of the Americas, New York, NY 10010

0142-727X/97/$17.00
PII S0142-727X(97)00007-6

when it reaches a critical value. Physically, those turning points indicate the stability limits of drops stressed by an electric field. No steady solution can be obtained if the externally applied electric field is increased beyond the critical field strength. However, in some special cases with fluid conductivities closely matched, they found that the drop deformations can grow indefinitely as the electric field strength increases. Therefore, with closely matched fluid electrical conductivities very large drop deformations are possible without becoming unstable. Feng and Scott also found that the deformed drop shapes are very nearly spheroidal for moderate drop deformations. In this paper, we analyze the effect of drop deformation on the heat transport to a drop suspended in uniform electric field. We assume the drop shape to be spheroid. A range of deformations from nearly spherical ($b/a = 0.99$) to disc-like ($b/a = 0.4$) are considered, where $2a$ is the length of the drop major axis and $2b$ is the drop minor axis. The assumption of a spheroid drop shape reduces the computational efforts considerably with little loss of accuracy. The electric field and the resulting flow field are numerically calculated in the continuous and the dispersed phase. The transient temperature variation and the Nusselt number variations are numerically obtained in the limit of bulk of the resistance to the heat transport being in the drop. Results indicate that the increase in drop deformation leads to higher heat transport to the drop in the limit of very large and very small Peclet numbers. However, for moderate equivalent Peclet numbers, the equivalent Nusselt numbers for a deformed drop are smaller than those for a liquid sphere.

Problem formulation

Consider a drop of a dielectric liquid suspended in another dielectric liquid. Application of a uniform electric field to such a system results in development of stresses on the surface of the drop. The nonuniform shear stress at the droplet surface results in a circulatory motion inside the drop. In general, the nonuniformity in the normal stress at the drop surface leads to deformation of the drop. Taylor (1966) showed analytically that for small deformations, the deformed drop shape is a spheroid. Numerous experimental studies (Allan and Mason 1962; Taylor 1966; Torza et al. 1971; Vizika and Saville 1992) have shown that the drop shape is very nearly spheroid, even for moderate deformations. We have considered the deformed drop shape as a spheroid. This simplification allows us to use an orthogonal coordinate system that conforms to the drop surface, thereby reducing the computational efforts with little loss of accuracy.

We note that both prolate and oblate drop deformations are possible and can be determined by Taylor's discriminating function:

$$\Phi = S(R^2+1) - 2 + 3(SR-1)\frac{2M+3}{5M+5} \tag{1}$$

$\Phi < 0$ indicates oblate deformations; whereas, $\Phi > 0$ results in prolate deformations. $\Phi = 0$ corresponds to a spherical drop. For most practical situations, it has been shown that prolate deformations will result when the drop is more conductive than the surrounding fluid, and oblate deformations are likely when the drop is less conductive than the surrounding fluid (Feng and Scott 1996). In situations involving heat/mass transport enhanced by application of electric field, it is found that significant enhancement is possible by keeping the ratio of the resistivity of the continuous phase to the resistivity of the drop phase as low as possible (Chang and Berg 1983). Therefore, oblate deformations of the drop are more likely in heat/mass transfer enhancement situations. It is also shown by Stewart and Morrison (1979) that inertial forces tend to produce oblate deformations for a moving drop. In view of the above considerations, we have considered oblate drop deformations in this paper. However, the model formulated here can also be applied to a prolate drop.

Notation

a	half of drop major diameter
A_s	drop surface area
b	half of drop minor diameter
E	electric field
i	unit vector
k	dielectric constant
M	viscosity ratio (μ_1/μ_2)
Nu	Nusselt number based on drop major diameter, Equation 18
p	pressure
Pe	Peclet number based on drop major diameter
$\widehat{Nu}$	equivalent Nusselt number defined in Equation 21
$\widehat{Pe}$	equivalent Peclet number defined in Equation 20
Q	heat flux
R	electric conductivity ratio (σ_1/σ_2)
Re	Reynolds number
(r, z, θ)	cylindrical polar coordinates
S	ratio of dielectric constants (k_1/k_2)
t	time
T	temperature
u	velocity
U	maximum surface velocity
V	electric potential
$\hat{V}$	volume
w	vorticity

Greek

α	thermal diffusivity
γ	surface tension
μ	viscosity
ρ	density
σ	electric conductivity
τ	stress
ψ	stream function
Φ	Taylor's discriminating function, Equation 1
(ξ, η, ϕ)	oblate spheroidal coordinates

Subscripts

0	initial
1	continuous phase
2	dispersed phase
b	bulk
E	electrically induced
s	surface
∞	far field

Superscript

*	dimensional quantities

Calculation of the electric field and the resulting flow field

We consider a drop of leaky dielectric fluid suspended in another dielectric fluid. The dispersed phase is denoted by subscript 2, and the continuous phase is denoted by subscript 1. The formulation is axisymmetric. The electric field is uniform far from the drop. The electric field in both the phases can be calculated by the Laplace's equation, and the flow is described by the Navier–Stokes equations.

$$\nabla \cdot \mathbf{u}_i^* = 0 \tag{2}$$

$$\mathbf{u}_i^* \cdot \nabla \mathbf{u}_i^* = -\frac{1}{\rho_i}\nabla p_i^* + \nu_i \nabla^2 \mathbf{u}_i^* \tag{3}$$

$$\nabla \cdot \mathbf{E}_i^* = 0 \tag{4}$$

where $\mathbf{E}^* = -\nabla V^*$ and $i = 1,2$.

At the interface the following conditions are satisfied (Melcher and Taylor 1969)

$$\begin{aligned} \mathbf{n}\cdot\mathbf{u}_i^* &= 0 \\ \mathbf{u}_1^* &= \mathbf{u}_2^* \\ \mathbf{n}\cdot(\tau_E^* + \tau_1^* - \tau_2^*) &= \tau_\gamma^* \\ V_1^* &= V_2^* \\ \sigma_1 \mathbf{n}\cdot\nabla V_1^* &= \sigma_2 \mathbf{n}\cdot\nabla V_2^* \end{aligned} \tag{5}$$

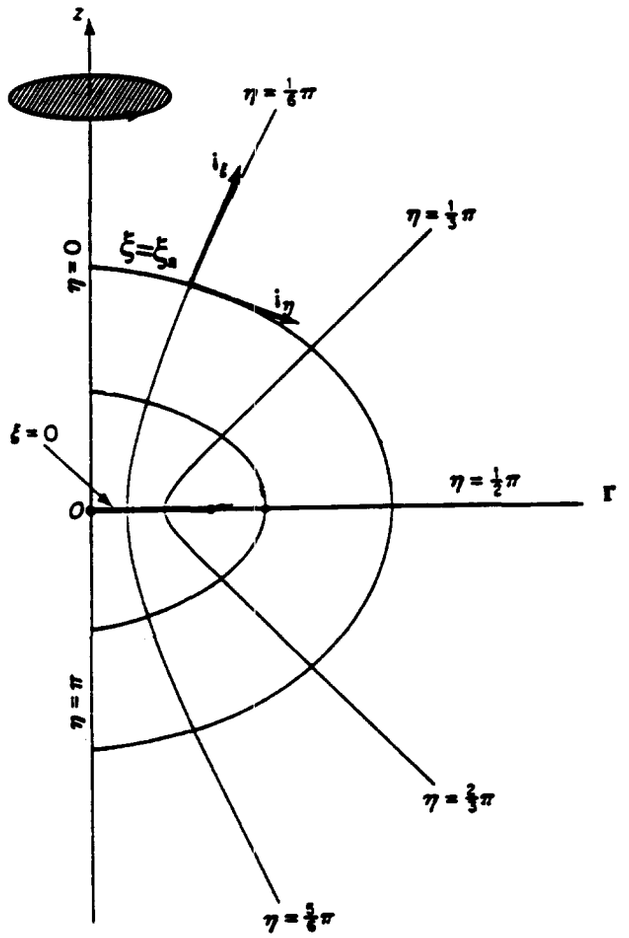

Figure 1 Oblate spheroidal coordinate system

Here τ_E is the electrically induced stress at the drop surface, τ_γ is the stress due to surface tension, and $\mathbf{n}$ is unit vector normal to the drop surface.

The symmetry condition is used along the axis of symmetry and far away from the drop we have

$$\mathbf{u}^* \to 0, \qquad p^* \to p_\infty^*, \qquad \text{and} \qquad V^* \to E^* z \tag{6}$$

We use the oblate spheroid coordinates (ξ, η, ϕ) for computational convenience. The origin of the coordinate system is at the drop center, as shown in Figure 1. The drop surface corresponds to $\xi = \xi_a$. The oblate spheroid coordinates are related to the cylindrical polar coordinates (r, z, θ) as (Happel and Brenner 1965)

$$\begin{aligned} z &= c \sinh\xi \cos\eta \\ r &= c \cosh\xi \sin\eta \\ \theta &= \phi \end{aligned} \tag{7}$$

The governing equations are made dimensionless as follows. Velocity is made dimensionless by the maximum surface velocity U, and distances are nondimensionalized by a. The stresses and pressure are normalized by $\mu U/a$, and the Reynolds number is $\mathrm{Re} = \rho U\, 2a/\mu$. The electric field is made dimensionless by $[\mu_2 U/(\epsilon_0 a)]^{1/2}$. We introduce stream function ψ (nondimensionalized by Ua^2) so that

$$u_\xi = -\frac{\cosh^2\xi_a}{(\cosh^2\xi - \sin^2\eta)^{1/2}\cosh\xi\sin\eta}\frac{\partial\psi}{\partial\eta} \tag{8}$$

$$u_\eta = \frac{\cosh^2\xi_a}{(\cosh^2\xi - \sin^2\eta)^{1/2}\cosh\xi\sin\eta}\frac{\partial\psi}{\partial\xi} \tag{9}$$

and vorticity $\mathbf{w}$ (nondimensionalized by U/a) as

$$\mathbf{w} = \nabla \times \mathbf{u} \tag{10}$$

In this axisymmetric formulation, only the ϕ component of vorticity is nonzero. Therefore, we have $\mathbf{w} = w\mathbf{i}_\phi$. The governing equations can now be written as

$$\begin{aligned} &\frac{\partial}{\partial\xi}\left(-\cosh\xi_a\frac{\partial\psi}{\partial\eta}w\right) + \frac{\partial}{\partial\eta}\left(\cosh\xi_a\frac{\partial\psi}{\partial\xi}w\right) \\ &\quad - \frac{2}{\mathrm{Re}}\left\{\frac{\partial}{\partial\xi}\left(\cosh\xi\sin\eta\frac{\partial w}{\partial\xi}\right) + \frac{\partial}{\partial\eta}\left(\cosh\xi\sin\eta\frac{\partial w}{\partial\eta}\right)\right\} \\ &\quad = w\left[-\tanh\xi\frac{\partial\psi}{\partial\eta}\cosh\xi_a + \cot\eta\frac{\partial\psi}{\partial\xi}\cosh\xi_a \right. \\ &\quad \left. - \frac{2}{\mathrm{Re}}\left(-\frac{\sin\eta}{\cosh\xi} + \frac{\cosh\xi}{\sin\eta}\right)\right] \end{aligned} \tag{11}$$

$$\begin{aligned} &\frac{\partial}{\partial\xi}\left(\frac{1}{\cosh\xi\sin\eta}\frac{\partial\psi}{\partial\xi}\right) + \frac{\partial}{\partial\eta}\left(\frac{1}{\cosh\xi\sin\eta}\frac{\partial\psi}{\partial\eta}\right) \\ &\quad = (\cosh^2\xi - \sin^2\eta)\mathrm{sech}^3\xi_a w \end{aligned} \tag{12}$$

$$\frac{\partial}{\partial\xi}\left(\cosh\xi\sin\eta\frac{\partial V}{\partial\xi}\right) + \frac{\partial}{\partial\eta}\left(\cosh\xi\sin\eta\frac{\partial V}{\partial\eta}\right) = 0 \tag{13}$$

The boundary conditions are: as $\xi \to \infty$, u_ξ, $u_\eta = 0$ and $w = 0$. The interface conditions at $\xi = \xi_a$ are:

$$\tau_{E,\xi\eta} + \frac{\mu_1}{\mu_2}\tau_{1,\xi\eta} - \tau_{2,\xi\eta} = 0$$

$$u_{1,\eta} = u_{2,\eta}$$

$$u_{1,\xi} = u_{2,\xi} = 0$$

$$\frac{\partial V_1}{\partial \xi} = \frac{\sigma_2}{\sigma_1}\frac{\partial V_2}{\partial \xi}$$

$$V_1 = V_2 \tag{14}$$

The shear stress can be written as

$$\tau_{\xi\eta} = \frac{1}{(\cosh^2\xi - \sin^2\eta)^{1/2}}\left\{\left[\frac{\partial u_\eta}{\partial \xi} + \frac{\sin\eta\cos\eta}{(\cosh^2\xi - \sin^2\eta)}u_\xi\right] + \left[\frac{\partial u_\xi}{\partial \eta} - \frac{\sinh\xi\cosh\xi}{(\cosh^2\xi - \sin^2\eta)}u_\eta\right]\right\}$$

$$\tau_{E,\xi\eta} = (k_1 E_{1,\eta} E_{1,\xi} - k_2 E_{2,\eta} E_{2,\xi})$$

As a consequence of the assumed oblate spheroid shape of the drop, the interfacial condition of normal stress balance need not be considered further.

Transient heat transfer

We investigate the transient heat transport in the drop interior when the drop is suddenly exposed to a step change in surface temperature. We consider that the bulk of the resistance to the heat transfer is in the droplet. Therefore, the drop surface temperature corresponds to the free-stream temperature. The flow field is considered fully developed and steady. The temperature in the drop interior can be calculated by the solution of energy conservation equation.

$$\frac{\partial T_2^*}{\partial t^*} + \mathbf{u}^* \cdot \nabla T_2^* = \alpha_2 \nabla^2 T_2^* \tag{15}$$

We define the dimensionless temperature as $T = (T_2^* - T_s^*)/(T_{2,0}^* - T_s^*)$ and dimensionless time as $t = \alpha_2 t^*/a^2$. The Peclet number is given by $\mathrm{Pe} = 2Ua/\alpha_2$. The governing equation and the boundary conditions in terms of the dimensionless variables can be written as follows.

$$\frac{(\cosh^2\xi - \sin^2\eta)\cosh\xi\sin\eta}{\cosh^3\xi_a}\frac{\partial T}{\partial t} + \frac{\mathrm{Pe}}{2}\left[\frac{\partial}{\partial \xi}\left(-\frac{\partial \psi}{\partial \eta}T\right) + \frac{\partial}{\partial \eta}\left(\frac{\partial \psi}{\partial \xi}T\right)\right] - \operatorname{sech}\xi_a\left[\frac{\partial}{\partial \xi}\left(\cosh\xi\sin\eta\frac{\partial T}{\partial \xi}\right) + \frac{\partial}{\partial \eta}\left(\cosh\xi\sin\eta\frac{\partial T}{\partial \eta}\right)\right] = 0 \tag{16}$$

Boundary conditions and initial conditions are:

$$\frac{dT}{d\eta} = 0 \quad \text{at} \quad \eta = 0, \pi$$

At the interface

$$\xi = \xi_a, \quad T = 0$$

At

$$t = 0, \quad T = 1 \tag{17}$$

The Nusselt number based on the drop major diameter is

$$\mathrm{Nu} = \frac{Q\,2a}{A_s(T_s^* - T_b^*)k} \tag{18}$$

$$= -\frac{2\hat{V}}{A_s a}\frac{1}{T_b}\frac{dT_b}{dt} \tag{19}$$

Here, Q is the net rate of heat transport to the drop, $\hat{V}$ is the volume of the drop $\hat{V} = \frac{4}{3}\pi a^2 b$, and A_s is the drop surface area

$$A_s = \int_0^\pi 2\pi\cosh\xi_a \sin\eta(\cosh^2\xi_a - \sin^2\eta)^{1/2}\,d\eta$$

The dimensionless bulk temperature can be calculated as

$$T_b = \frac{3}{2}\frac{1}{\sinh\xi_a\cosh^2\xi_a} \times \int_0^{\xi_a}\int_0^\pi T\cosh\xi\sin\eta(\cosh^2\xi - \sin^2\eta)\,d\eta\,d\xi$$

Numerical methodology

Equations 11–13 and Equation 16 are solved with the appropriate boundary conditions (Equations 14 and 17) using a finite-difference method. All the equations are discretized using central differencing. In the drop interior, 61×61 node points were used and 101×61 node points were used in the surrounding fluid. The electric field is first calculated for each drop deformation. Electric potential is specified in the far field ($\xi = \xi_\infty$). The value of ξ_∞ is chosen so that the distance between any point on the far-field boundary and the drop surface is at least $100a$. To study the effect of finiteness of the far-field boundary, solution for electric potential was obtained for a deformed drop with $b/a = 0.7$ by considering the far-field boundary at $200a$. The change in the surface potential and surface potential gradients were less then 1%. The electric potential in the dispersed and the continuous phase was obtained by the following iterative procedure. A guess value of the electric potential at the drop surface is specified to calculate the electric field in the continuous phase. The electric potential gradient along the drop surface obtained from the solution to the continuous phase is used as a boundary condition to solve for the electric potential distribution inside the drop. The improved surface potential variation is then used as a boundary condition for the solution in the continuous phase. The iterations are continued until the variation in the electric potential between successive iterations is less than 10^{-6}. The governing equations for the stream function and vorticity transport were solved in both phases by an iterative procedure. Note that the maximum value of the tangential velocity at the drop surface must be unity by virtue of the nondimensionalization scheme.

The solution to the flow field provides the nondimensional velocity distribution on the drop surface. The electric field distribution is then updated so that the maximum dimensionless velocity on the drop surface equals unity. Most of the numerical calculations were performed with $R = 0.1$, and $S = 2$. Note that for a known drop shape, the particular choice of the R and S values affect the magnitude, but do not affect the angular variation, of the electrically induced stresses, provided R and S are not unity. ($R = S = 1$ gives a trivial solution of zero interfacial stresses.) For example, for a liquid sphere ($b/a = 1$), $\tau_{E,\eta\zeta}/\tau_{E,\eta\xi,\max} = 2 \sin\eta \cos\eta$, irrespective of the particular values of R and S (Taylor 1966). Therefore, a change in R and S will change the value of the electric field that corresponds to a nondimensional maximum surface velocity of unity, but will not affect the dimensionless flow field. Therefore, applicability of the results obtained in this study is not limited to the particular values of the parameters R and S used in our computations.

Transient temperature distributions inside the droplet were obtained for Peclet numbers from 5 to 1500. Alternating direction implicit method with a tridiagonal algorithm was employed to solve the energy equation. The time-step was varied from 0.00001 for short times to 0.0001 at large t. For a typical run, the solution of electric field and the resulting flow field took less than 1 hour on a HP 9000/712/80 workstation. The solution to the energy equation required from 10 minutes (high Pe) to 30 minutes (low Pe). To study the effect of grid refinement, results for Pe = 200 and $b/a = 0.7$ were also obtained with doubling the node points in each direction. The change in the Nusselt number variation was found to be less than 2%.

Results and discussion

We have studied the effect of drop deformation on the heat transport in a drop suspended in a uniform electric field. A range of drop deformations is considered from $b/a = 0.99$ (approximate sphere) to $b/a = 0.4$ (disk-like). The transient heat transport is studied in the limit of bulk of the resistance to heat transfer being in the drop. Under this condition, the transport is governed by the drop Peclet number based on the maximum tangential velocity. A range of Peclet numbers from 5 to 1500 is considered. The numerical computations are carried out for a suspended drop ($\rho_1/\rho_2 = 1$). We have used $\mu_1/\mu_2 = 1$ in our computations. For one of the cases (Pe = 200 and $b/a = 0.7$), the calculations were also carried out by varying the viscosity ratio to 0.1 and 5. The heat transfer results remained essentially unchanged. In all of the earlier studies on heat transfer in a spherical drop suspended in uniform electric field, the assumption of Stokes flow (Re $\ll 1$) has been used. To make fruitful comparisons with the available results, we have used a value of drop Reynolds number as 0.1 in our computations.

The flow field inside and outside the drop is shown in Figures 2 and 3 for $b/a = 0.99$ and 0.7, respectively. As expected, the streamline distribution is symmetric about the equatorial plane. The negative values of the stream function in the upper half of the drop interior indicate that the flow in the lower half moves in a direction opposite to that of the upper half. The flow on the drop surface is from the poles to the equator. With increasing drop deformation, the center of each circulatory vortex pattern moves toward the equatorial plane. The radial distance of the vortex center from the drop surface is substantially less for a drop with $b/a = 0.7$, as compared to that for a liquid sphere. The electrically induced dimensionless surface velocities are shown in Figure 4 for three drop deformations. For a liquid sphere $b/a = 0.99$, the maximum velocity (magnitude) occurs at $\eta = \pi/4$, $3\pi/4$. As the drop deformation is increased, the location of maximum velocity shifts toward the equator. The dotted line shows the analytical results of Taylor (1966) for the surface velocity variation for a liquid sphere. It can be seen that our results for a sphere are in excellent agreement with the analytical solution.

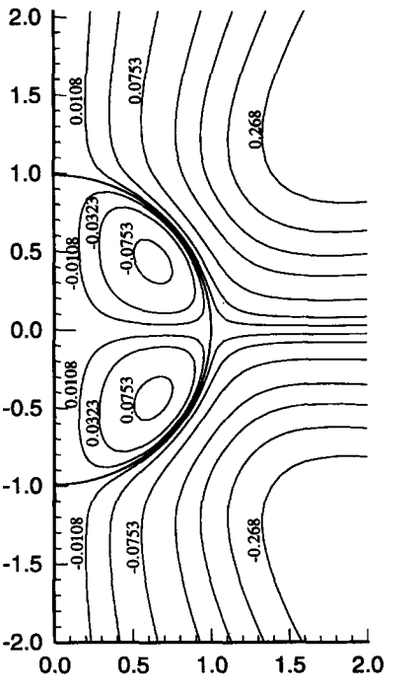

Figure 2 Streamlines in the drop interior for a spherical drop ($b/a = 0.99$); $R = 0.1$; $S = 2$, $E = 12.4$.

The transient Nusselt number variation are shown in Figure 5 for a range of Peclet numbers for a "sphere." The corresponding variations of drop bulk temperature are shown in Figure 6. Figure 5 is also a comparison of our results with those of Oliver et al. (1985) for a liquid sphere. The comparison shows that the

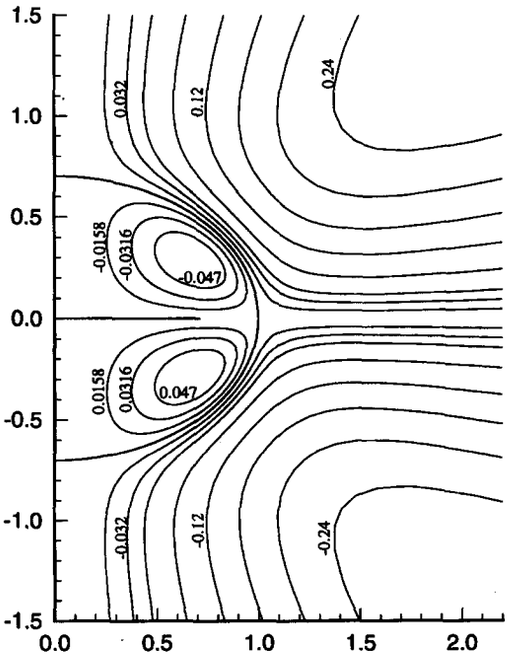

Figure 3 Streamlines in the drop interior for a deformed drop with $b/a = 0.7$; $R = 0.1$; $S = 2$, $E = 21.98$

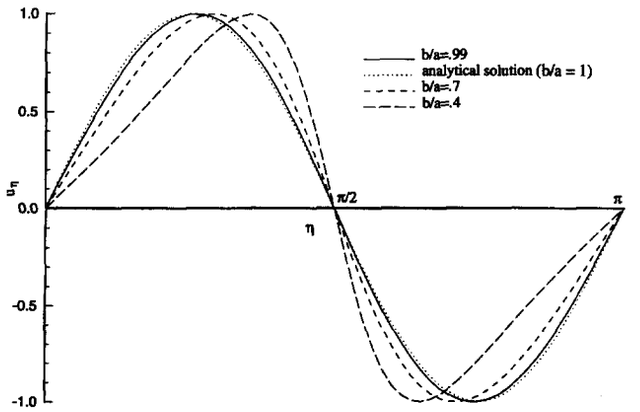

Figure 4 Nondimensional velocity variation on the drop surface; legend: solid lines—calculated results for a sphere; dotted line—analytical solution for a liquid sphere; dashed lines—results for deformed drops

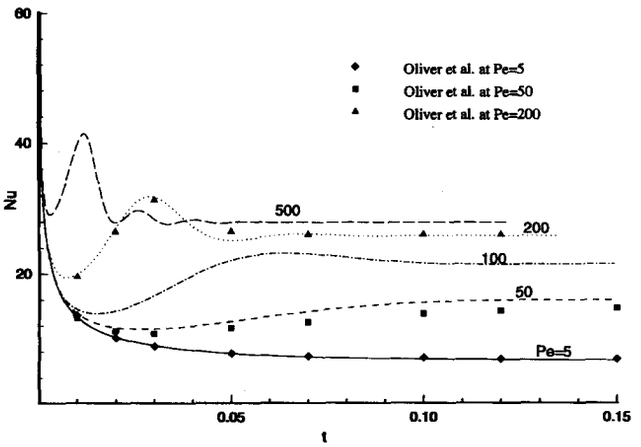

Figure 5 Nusselt number variation for a sphere ($b/a=0.99$): comparison with results of Oliver et al. (1985).

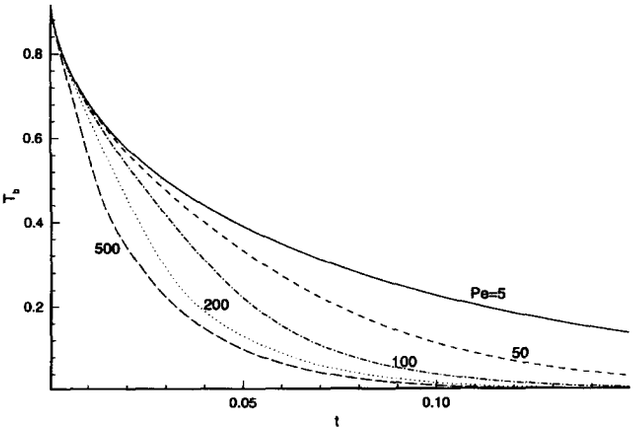

Figure 6 Dimensionless bulk temperature variation with time for a liquid sphere

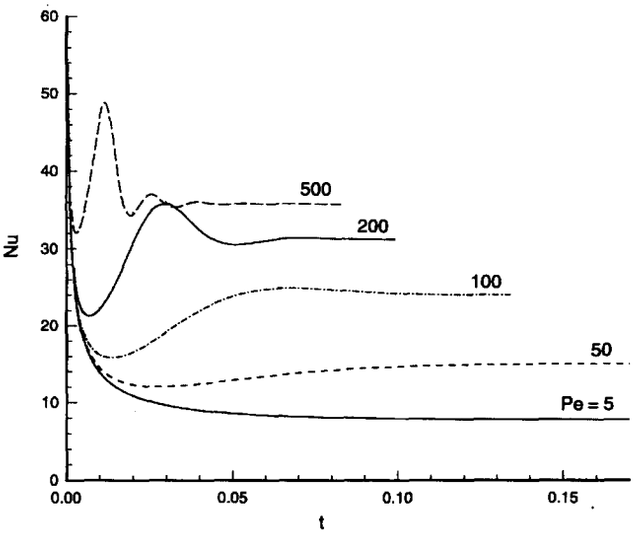

Figure 7 Variation of Nusselt number (based on drop major diameter) for a deformed drop with $b/a=0.7$

transient Nusselt number variations calculated from our model match well with the results of Oliver et al. In the limit of negligible drop deformation, our results for the surface velocities, the flow field, and the heat transport are in excellent agreement with those for a sphere. This can be considered to be a validation of our computational model. Figure 7 shows the transient Nusselt number variation for a deformed drop $b/a = 0.7$. For all Peclet numbers, for short times, conduction is the dominant heat transport mechanism, as can be seen from the sharp initial drop in the Nusselt number. This is caused by the steep temperature gradients near the drop surface. For low Peclet numbers, conduction remains to be the dominant mechanism at all times. For higher Peclet number, the Nusselt number decreases for short times, but starts increasing thereafter as the cold fluid from the drop interior is brought near the drop surface because of the circulatory motion. The Nusselt number oscillations are more pronounced for high Peclet numbers. The Nusselt number variation eventually attains a steady state. The steady-state Nusselt number value increases as the Peclet number is increased. The steady-state Nusselt number values become increasingly independent of the Peclet number for very large Peclet numbers. The bulk temperature variation with dimension-

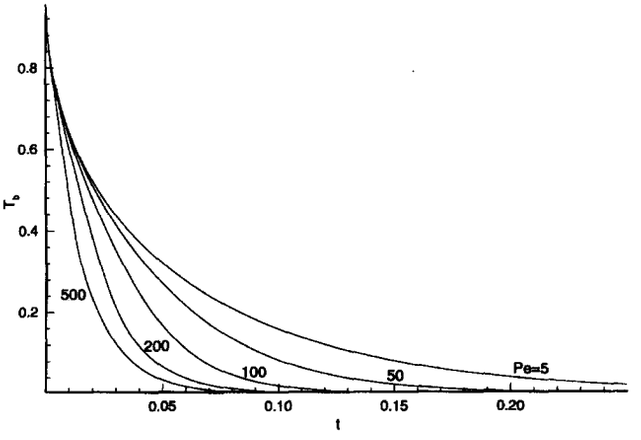

Figure 8 Temporal variation of dimensionless bulk temperature for a deformed drop with $b/a=0.7$

less time is shown in Figure 8 for $b/a = 0.7$. The dimensionless bulk temperature decreases rapidly for short times. The bulk temperature variations are qualitatively similar to those for a liquid sphere. The Nusselt number variation for a drop with $b/a = 0.4$ is shown in Figure 9. The corresponding bulk temperature variation is shown in Figure 10. The transient bulk temperature variations show that for higher Peclet numbers, the drop bulk temperature drops more rapidly than that for lower Peclet numbers for all drop deformations. The qualitative behavior of the Nusselt number variation is similar to that obtained for a liquid sphere (Chung and Oliver 1990). However, for large Peclet numbers, the steady-state Nusselt number values are significantly higher for a deformed drop than those for a sphere.

We note that the Peclet number is based on the drop major diameter and the maximum surface velocity. Therefore, for a deformed drop, the Peclet number will be $(a/b)^{1/3}$ times that for a sphere of identical volume and identical maximum surface velocity. A better comparison of the steady-state Nusselt numbers can be carried out by defining an equivalent Peclet number and an equivalent Nusselt number for a deformed drop as

$$\widehat{\mathrm{Pe}} = \frac{U\,2r}{\alpha_2} = \mathrm{Pe}\left(\frac{b}{a}\right)^{1/3} \tag{20}$$

$$\widehat{\mathrm{Nu}} = \mathrm{Nu}\left(\frac{b}{a}\right)^{1/3} \tag{21}$$

where r is the radius of a sphere of equal volume as the deformed drop, $r = a^{2/3}b^{1/3}$.

Figure 11 shows the variations of equivalent steady-state Nusselt numbers with equivalent Peclet numbers. In the limit of small equivalent Peclet number, the equivalent Nusselt numbers are higher for a deformed drop than those for a liquid sphere. In this range of small $\widehat{\mathrm{Pe}}$, conduction is the dominant mechanism of heat transport in the drop. Conduction of heat in a deformed drop is much faster than that in a sphere because of the smaller length scale and greater surface area for a deformed drop. In the limit of small b/a, heat conduction length scale for a deformed drop is b. This is much smaller than a radius of a sphere of identical volume $r = a^{2/3}b^{1/3}$. Therefore, for small Peclet numbers, the Nusselt numbers for a deformed drop is higher than those for a spherical drop.

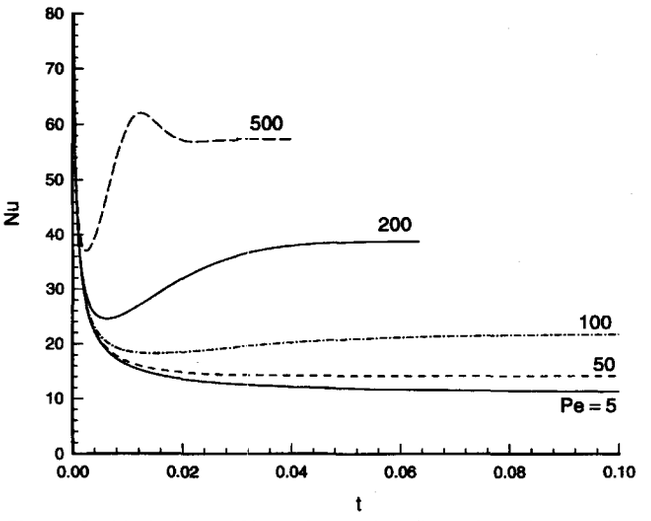

Figure 9 Variation of Nusselt number (based on drop major diameter) for a deformed drop with $b/a = 0.4$

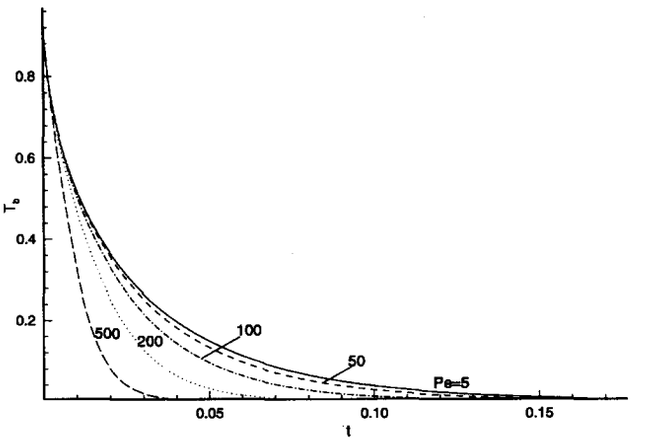

Figure 10 Temporal variation of dimensionless bulk temperature for a deformed drop with $b/a = 0.4$

It is evident from the flow streamlines shown in Figures 2 and 3 that the center of the vortex for a deformed drop is situated near the equator and closer to the drop surface than that for a sphere. At moderate Peclet number, the circulatory vortex in a deformed drop is, therefore, less effective in bringing the cold fluid from drop interior to near the drop surface. Hence, at moderate Peclet numbers, it is observed that the Nusselt numbers for a deformed drop are lower than those for a sphere.

At very large Peclet numbers, convection is the most dominant transport mechanism and the temperature gradients along each stream line diminish quickly. Therefore, after the initial transients, the heat transport is mainly in the direction perpendicular to the streamlines. For a given Peclet number, the resistance to the heat transport perpendicular to the stream lines will be inversely proportional to the distance between the drop surface and the center of the vortex. This distance is much smaller in the case of deformed drop than that for sphere. This results in higher Nusselt numbers for deformed drops at high Peclet numbers.

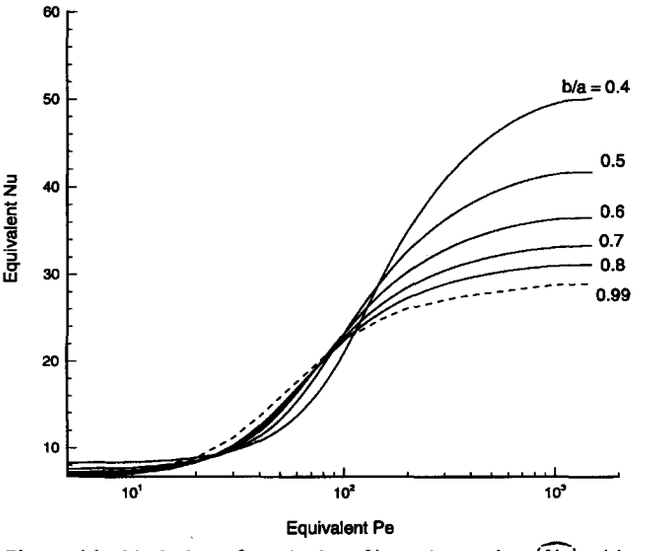

Figure 11 Variation of equivalent Nusselt number $(\widehat{Nu})$ with equivalent Peclet number $(\widehat{Pe})$ for deformed drops

Conclusions

We have studied the transient heat transport in a deformed drop suspended in a uniform electric field by numerical methods. The governing equation for the electric potential is solved to obtain the electrically induced stresses at the drop surface. The resulting flow field is determined by solving a stream function—vorticity formulation in the dispersed and the continuous phase. The results for the transient temperature distribution and the Nusselt number are obtained in the limit of bulk of the resistance to the heat transport being in the drop. Results show that the location of maximum surface velocity moves toward the equatorial plane with increasing drop deformation. For all drop deformations, the steady-state Nusselt numbers become increasingly independent of Peclet number for large Peclet number. The steady-state Nusselt numbers for a deformed drop are higher than that for sphere for very low and very high Peclet numbers. However, for intermediate range of Peclet numbers, the steady-state Nusselt number for a deformed drop may be lower than that for a liquid sphere. The maximum steady-state Nusselt number increases as the drop deformation is increased.

Acknowledgments

Support for this work by the National Science Foundation under Grant CTS-9409140 is gratefully acknowledged. Partial funding for numerical computations was provided by the University of Cincinnati, Cincinnati, Ohio.

References

Allan, R. S. and Mason, S. G. 1962. Particle behavior in shear and electric fields I. Deformation and burst of fluid drops. Proc. R. Soc., **267 A,** 45–61

Ayyaswamy, P. S. 1995. Direct-contact transfer process with moving liquid droplets. In Advances in Heat Transfer, Vol. 26, J. P. Hartnett and T. F. Irvine (eds.), Academic Press, San Diego, CA, 1–104

Chang, L. S. and Berg, J. C. 1983. Fluid flow and transfer behavior of a drop translating in an electric field at intermediate Reynolds number. Int. J. Heat Mass Transfer, **26,** 823–832

Chung, J. N. and Oliver, D. L. R. 1990. Transient heat transfer in a fluid sphere translating in an electric field. J. Heat Transfer, **112,** 84–91

Clift, R., Grace, J. R. and Weber, M. E. 1978. Bubbles, Drops, and Particles, Academic Press, San Diego, CA, chapter 7

Feng, J. Q. and Scott, T. C. 1996. A computational analysis of electrohydrodynamics of a leaky dielectric drop in an electric field. J. Fluid Mech., **311,** 289–326

Happel, J. and Brenner, H. 1965. Low Reynolds Number Hydrodynamics, Noordhoff, Leyden, The Netherlands

Jog, M. A., Ayyaswamy, P. S., and Cohen, I. M. 1996. Evaporation and combustion of a slowly moving liquid fuel droplet: Higher-order theory. J. Fluid Mechanics, **307,** 135–165

Melcher, J. R. and Taylor, G. I. 1969. Electrohydrodynamics: a review of the role of interfacial shear stresses. Ann. Rev. Fluid Mech., **1,** 111–146

Oliver, D. L. R., Carleson, T. E., and Chung, J. N. 1985. Transient heat transfer to a fluid sphere suspended in an electric field. Int. J. Heat Mass Transfer, **28,** 1005–1009

Oliver, D. L. R. and DeWitt, K. J. 1993. High Peclet number heat transfer from a droplet suspended in an electric field: Interior problem. Int. J. Heat Mass Transfer, **36,** 3153–3155

Sadhal, S. S. and Johnson, R. E. 1986. On the deformation of drops and bubbles with varying interfacial tension. Chem. Eng. Comm., **46,** 97–109

Stewart, M. B. and Morrison, F. A. 1979. Small Reynolds number electro-hydrodynamic flow around drops and the resulting deformation. J. Appl. Mech., **46,** 510–512

Taylor, G. I. 1966. Studies in electrohydrodynamics, I. The circulation produced in a drop by an electric field. Proc. R. Soc., **291 A,** 159–166

Torza, S., Cox, R. G., and Mason, S. G. 1971. Electrohydrodynamic deformation and burst of liquid drops. Phil. Trans. R. Soc. London A, **269,** 295–319

Vizika, O. and Saville, D. A. 1992. The electrohydrodynamic deformation of drops suspended in liquids in steady and oscillatory electric fields. J. Fluid Mech., **239,** 1–21